JOURNAL OF MATERIALS SCIENCE **36** (2001) 255–261

Analyses of thermal expansion behavior of intergranular two-phase composites

C. H. HSUEH, P. F. BECHER, E. Y. SUN
Metals and Ceramics Division, Oak Ridge National Laboratory, Oak Ridge, Tennessee 37831-6068, USA
E-mail: hsuehc@ornl.gov

Both analytical modeling and numerical simulations were performed to analyze residual thermal stresses and coefficients of thermal expansion (CTEs) of intergranular two-phase composites in a two-dimensional sense. A composite-circle model was adopted for analytical modeling. Model microstructures consisting of square-array, hexagon-array, and brick wall-array of grains with an intergranular phase as well as an actual microstructure of random-array grains with an intergranular phase were adopted for numerical simulations. The results showed that in predicting CTEs, the simple analytical model represents the two-dimensional composite well except that with brick wall-array grains, which induced significant anisotropic CTEs in the composite. The residual thermal stresses in composites were also discussed. © *2001 Kluwer Academic Publishers*

1. Introduction

Two-phase microstructures offer some unique opportunities for improving mechanical properties of structural ceramic materials [1]. Since the two phases have different thermal-mechanical properties, residual thermal stresses develop during cooling of the composite from its fabrication temperature. These residual thermal stresses can, in some instances, result in toughening effects for particle-reinforced ceramic composites [2–4]. To analyze these toughening effects, an understanding of the residual thermal stress distributions in the composite is required. Also, the thermal expansion behavior of the composite is affected by the existence of residual thermal stresses. While the thermal expansion behavior of composites can be characterized by their effective coefficients of thermal expansion (CTEs) [5–9], these effective CTEs are inevitably functions of residual thermal stresses and hence of the microstructures of composites. However, the relationship between effective CTEs and microstructures of composites has not been systematically studied.

The purpose of the present study was to examine residual thermal stresses and effective CTEs of intergranular two-phases composites in a two-dimensional sense. First, analytical modeling was performed by using a simple composite-circle model to represent the intergranular two-phase composite. Then, a recently developed object oriented finite element analysis (*OOF*) [10] was adopted for numerical simulations. *OOF* is uniquely designed to operate on microstructural images, and thus can incorporate the actual microstructure. Model microstructures of square-array, hexagon-array, and brick wall-array grains with an intergranular phase as well as an actual microstructure were adopted for simulations. Whereas square-array and hexagon-array grains simulate equilateral grains, brick wall-array grains simulate aligned elongated grains. The actual microstructure has a random distribution of grains. The distributions of residual thermal stresses in each system were discussed, and the effective CTEs obtained from numerical simulations were compared to those predicted from analytical modeling. The physical meaning of the deviation of the effective CTEs from the rule-of-mixtures CTE for two-phase composites was also discussed.

2. Analytical modeling

For an intergranular two-phase composite, a composite-circle (Fig. 1) can be used as the representative volume element in a two-dimensional sense such that the inner circle and the outer annulus represent the grain and the intergranular phase, respectively. Fig. 1 shows that a circular region of phase 1 with a radius a is surrounded by a concentric annulus of phase 2 with an outer radius b, such that a^2/b^2 corresponds to the area fraction of phase 1 in the composite. Residual thermal stresses develop during the temperature change in the system because of the thermal-mechanical mismatch between the two phases. The stresses can be determined by the procedure of first allowing the two phases to exhibit unconstrained differential thermal strains during the temperature change. Then, a radial stress, σ_a, is placed at the interface to restore the displacement continuity at the interface.

With an interfacial stress, σ_a, the radial and the tangential stresses in phases 1 and 2, are [11]

$$\sigma_{1,\mathrm{r}} = \sigma_a \tag{1a}$$

$$\sigma_{1,\mathrm{t}} = \sigma_a \tag{1b}$$

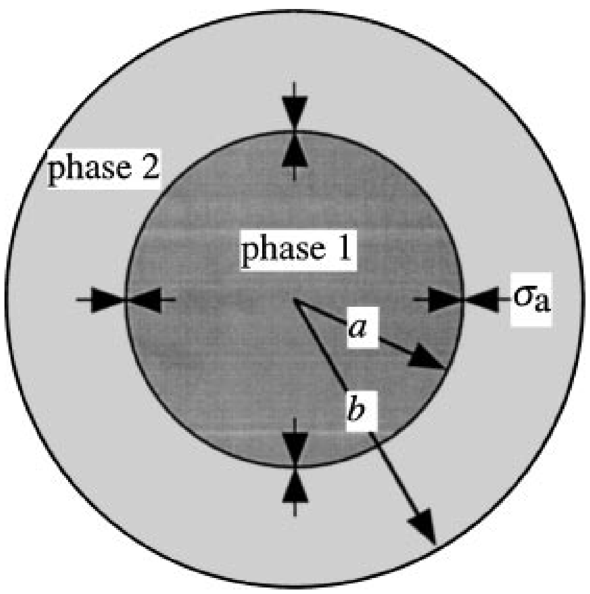

Figure 1 Schematic showing the composite-circle model for intergranular two-phase composites in a two-dimensional sense.

$$\sigma_{2,\mathrm{r}} = \frac{a^2(b^2 - r^2)\sigma_a}{r^2(b^2 - a^2)} \tag{2a}$$

$$\sigma_{2,\mathrm{t}} = \frac{-a^2(b^2 + r^2)\sigma_a}{r^2(b^2 - a^2)} \tag{2b}$$

where r is the distance from the center of the composite-circle, the subscripts 1 and 2 denote phase 1 and phase 2, and the subscripts r and t denote the radial and the tangential components, respectively.

With a temperature change, ΔT, the strain consists of two components: the elastic strain and the unconstrained thermal strain. The tangential strains in phases 1 and 2, $\varepsilon_{1,\mathrm{t}}$ and $\varepsilon_{2,\mathrm{t}}$, are respectively

$$\varepsilon_{1,\mathrm{t}} = \frac{\sigma_{1,\mathrm{t}} - \nu_1\sigma_{1,\mathrm{r}}}{E_1} + \alpha_1\Delta T \tag{3}$$

$$\varepsilon_{2,\mathrm{t}} = \frac{\sigma_{2,\mathrm{t}} - \nu_2\sigma_{2,\mathrm{r}}}{E_2} + \alpha_2\Delta T \tag{4}$$

where E, ν, and α are Young's modulus, Poisson's ratio, and the CTE, respectively.

The residual stresses in the system are contingent upon the solution of the interfacial stress, σ_a, which can be determined by the continuity condition at the interface. Continuity of the radial displacement at the interface is required. With the tangential strain proportional to the radial displacement, this continuity condition becomes

$$\varepsilon_{1,\mathrm{t}} = \varepsilon_{2,\mathrm{t}} \quad (\text{at } r = a) \tag{5}$$

Combination of Equations 1 through 5 yields

$$\sigma_a = \frac{(\alpha_2 - \alpha_1)\Delta T}{\frac{1-\nu_1}{E_1} + \frac{((b^2+a^2)/(b^2-a^2)) + \nu_2}{E_2}} \tag{6}$$

The stress invariant, $\sigma_\mathrm{r} + \sigma_\mathrm{t}$, can be obtained from Equations 1, 2, and 6, such that

$$\sigma_{1,\mathrm{r}} + \sigma_{1,\mathrm{t}} = \frac{2(\alpha_2 - \alpha_1)\Delta T}{\frac{1-\nu_1}{E_1} + \frac{((b^2+a^2)/(b^2-a^2)) + \nu_2}{E_2}} \quad (\text{in phase 1}) \tag{7}$$

$$\sigma_{2,\mathrm{r}} + \sigma_{2,\mathrm{t}} = \frac{-2a^2(\alpha_2 - \alpha_1)\Delta T}{\frac{(b^2-a^2)(1-\nu_1)}{E_1} + \frac{b^2+a^2+(b^2-a^2)\nu_2}{E_2}} \quad (\text{in phase 2}) \tag{8}$$

The deformation of the composite-circle during the temperature change is dictated by the radial displacement at $r = b$. Hence, the effective CTE of the composite-circle, α^*, is defined by $\varepsilon_{2,\mathrm{t}}$ at $r = b$, such that

$$\alpha^* = \frac{\varepsilon_{2,\mathrm{t}}}{\Delta T} \quad (\text{at } r = b) \tag{9}$$

Substitution of Equations 2, 4, and 6 into 9 yields

$$\alpha^* = \alpha_2 - \frac{2a^2(\alpha_2 - \alpha_1)}{(b^2 - a^2)\left[(1-\nu_1)\frac{E_2}{E_1} + \nu_2\right] + b^2 + a^2} \tag{10}$$

In the specific case of $E_1 = E_2$ and $\nu_1 = \nu_2$, Equations 10 becomes

$$\alpha^* = \alpha_\mathrm{rom} = \frac{a^2\alpha_1 + (b^2 - a^2)\alpha_2}{b^2} \tag{11}$$

Hence, when the two phases have the same elastic constants, the effective CTE of the composite can be obtained using rule of mixtures (rom).

Ignoring the difference in Poisson's ratio between the two phases and assuming $E_1 > E_2$, it can be obtained from Equations 10 and 11 that $\alpha^* < \alpha_\mathrm{rom}$ when $\alpha_1 < \alpha_2$, and $\alpha^* > \alpha_\mathrm{rom}$ when $\alpha_1 > \alpha_2$. Hence, α^* shifts from α_rom in the direction of the CTE of the harder phase.

3. Numerical simulations

Residual thermal stresses and effective CTEs of two-phase composites were numerically simulated using *OOF*, and the plane-stress case was considered. The simulations were conducted on both model microstructures and an actual microstructure. A two-dimensional uniform grid was used and each grid consisted of two triangular elements.* The micrographs were digitized to a portable pixel map (*ppm*) format, and each pixel corresponded to a grid. Hence, meshing in *OOF* is obtained simply by converting a micrograph to a *ppm* format. Therefore, the uniqueness of *OOF* is that it can operate directly on microstructural images. In the present study, each digitized micrograph consists of 64,800 elements. The thermal/mechanical properties used in the present numerical simulations are listed in Table I which are pertinent to the Si_3N_4/glass system [12] without considering the anisotropic properties

---

* An adaptive mesh was newly included in *PPM2OOF* which allows elements have different sizes at different parts of the system. The accuracy of the simulated results can be improved by using a higher resolution (i.e., more pixels) micrograph combined with adaptive meshing.

TABLE I The thermal-mechanical properties for intergranular two-phase composites

	Grain	Intergranular Phase
Young's Modulus, E (GPa)	380	145
Poisson's Ratio, ν	0.26	0.29
CTE ($\times 10^{-6}$/°C)	2.4	6

of Si_3N_4 grains. The temperature change, ΔT, used in calculating the thermal strain is -1000°C. However, the simulated results can be modified by noting that residual thermal stresses scale with ΔT and effective CTEs are independent of ΔT (providing that the temperature dependence of the CTEs of the composite constituents is not considered). The boundary of the micrograph is assumed to be free; however, the simulated results would be more meaningful if the periodic boundary condition (which will be implemented in *OOF* in the future) is used.

3.1. Residual stresses in model microstructures

Three model microstructures, square-array (Fig. 2a), hexagon-array (Fig. 3a), and brick wall-array (Fig. 4a) grains with intergranular phases, were analyzed in the present study. Both square-array and hexagon-array grains simulate equilateral grains. However, whereas residual thermal stress distributions and effective CTEs in the x- and y-directions are the same for square-array grains, they are different for hexagon-array grains. The brick wall-array grains simulate aligned elongated grains. Using *OOF*, the calculated stress maps for σ_x, σ_y, and the stress invariant, $\sigma_x + \sigma_y$, are shown in Figs 2–4 for the three model microstructures, respectively. The area fractions of the intergranular phase in model microstructures and the statistics of σ_x, σ_y, and $\sigma_x + \sigma_y$, in the grains and the intergranular phase are listed in Tables II and III, respectively. The stress invariants calculated from the analytical model are also listed in Tables II and III to compare with those from the numerical simulation having the same area fraction of the intergranular phase.

For square-array grains (Fig. 2a), the intergranular layers are oriented in either the x- or the y-direction. It can be seen in Fig. 2b that whereas σ_x is tensile in the intergranular layer parallel to the x-direction, it becomes compressive in the intergranular layer parallel to the y-direction. Similarly, whereas σ_y is tensile in the intergranular layer parallel to the y-direction, it

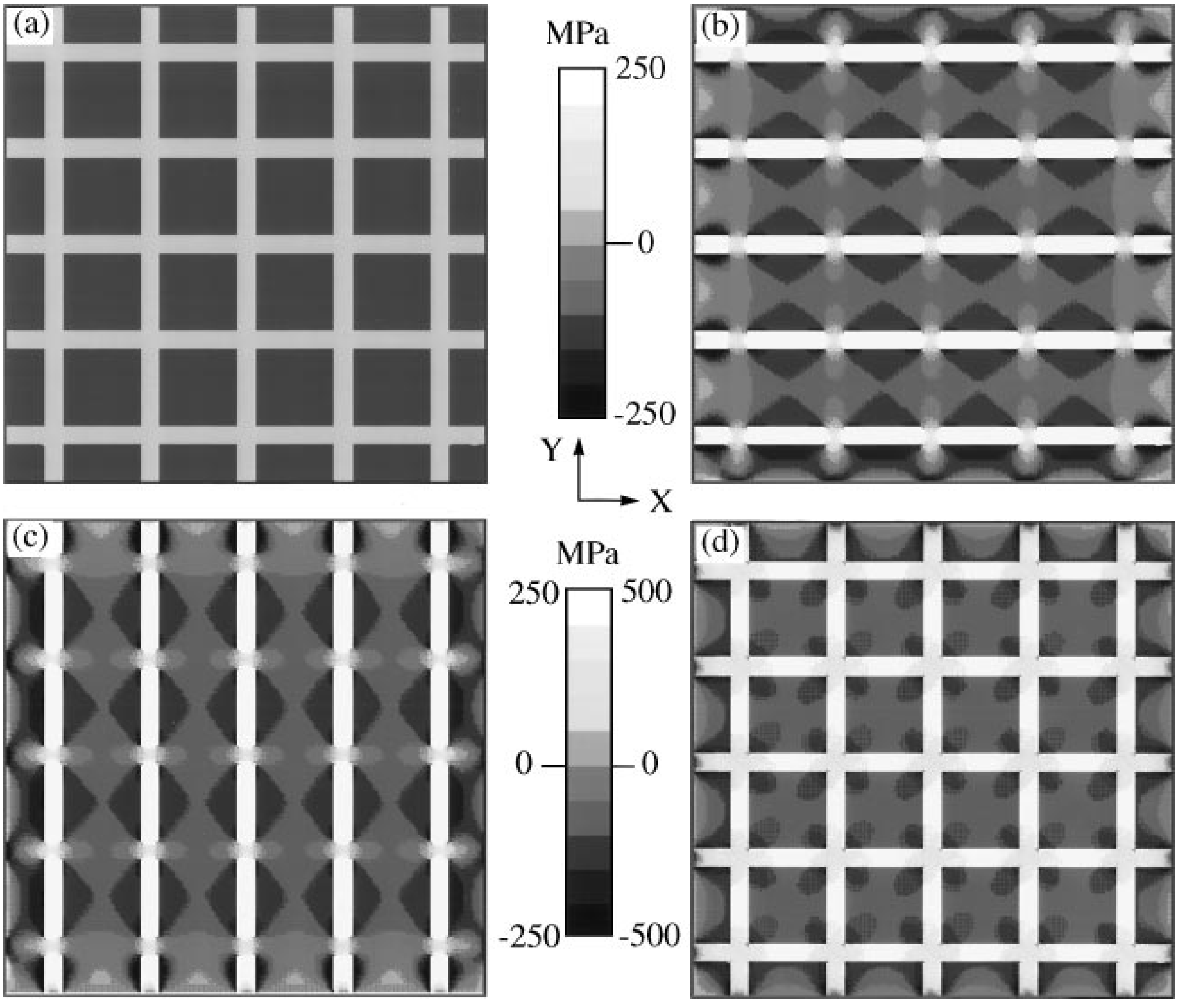

Figure 2 (a) The morphology, (b) residual thermal stress σ_x, (c) residual thermal stress σ_y, and (d) stress invariant, $\sigma_x + \sigma_y$, for square-array grains with an intergranular phase.

TABLE II The statistics of residual thermal stresses, σ_x and σ_y, and stress invariant, $\sigma_x + \sigma_y$, in grains for $\Delta T = -1000^\circ\mathrm{C}$

	Square (Fig. 2)	Hexagon (Fig. 3)	Brick wall (Fig. 4)	Random (Fig. 5)
Intergranular Phase Content	0.35	0.4	0.44	0.22
σ_x (MPa)	-94.3 ± 57.2	-108.3 ± 88.1	-244.9 ± 92.1	-85.1 ± 103
σ_y (MPa)	-94.3 ± 57.2	-115.5 ± 90.8	-37.7 ± 64.1	-71.7 ± 107.8
$\sigma_x + \sigma_y$ (MPa)	-142 ± 70	-166.8 ± 100.8	-266.2 ± 80.3	-161.4 ± 127.6
$\sigma_\mathrm{r} + \sigma_\mathrm{t}$ (MPa) Analytical Modeling	-197.5	-228.4	-253.6	-120.4

TABLE III The statistics of residual thermal stresses, σ_x and σ_y, and stress invariant, $\sigma_x + \sigma_y$, in the intergranular phase for $\Delta T = -1000^\circ\mathrm{C}$

	Square (Fig. 2)	Hexagon (Fig. 3)	Brick wall (Fig. 4)	Random (Fig. 5)
Intergranular Phase Content	0.35	0.4	0.44	0.22
σ_x (MPa)	174.4 ± 212.8	161.1 ± 156.7	313.8 ± 144.2	308.1 ± 181
σ_y (MPa)	174.4 ± 212.8	171.8 ± 172.7	48.3 ± 131.8	259.4 ± 189.6
$\sigma_x + \sigma_y$ (MPa)	378.1 ± 97.2	358.9 ± 98	374.6 ± 73.8	463 ± 100.9
$\sigma_\mathrm{r} + \sigma_\mathrm{t}$ (MPa) Analytical Modeling	366.7	342.5	322.7	427.3

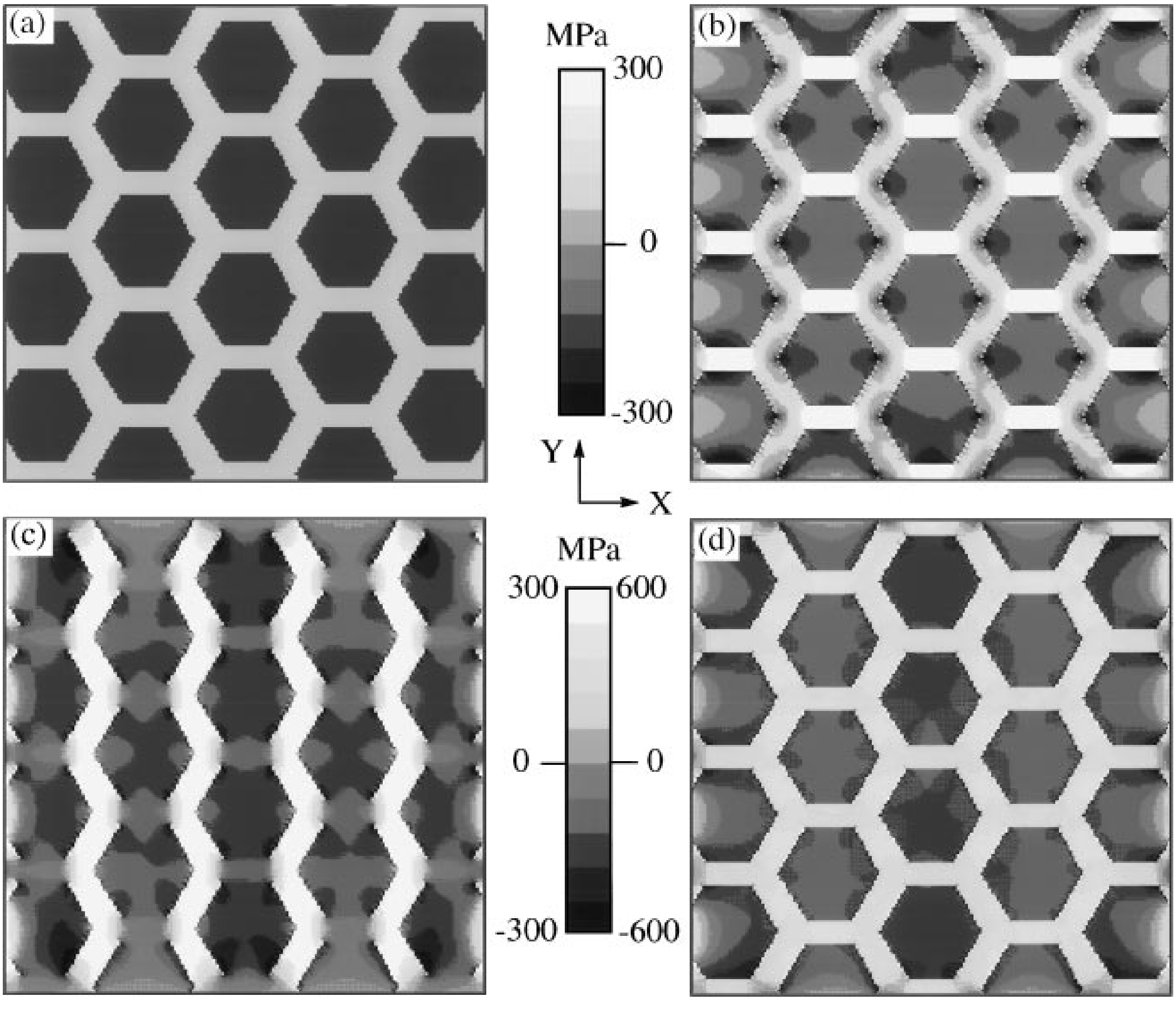

Figure 3 (a) The morphology, (b) residual thermal stress σ_x, (c) residual thermal stress σ_y, and (d) stress invariant, $\sigma_x + \sigma_y$, for hexagon-array grains with an intergranular phase.

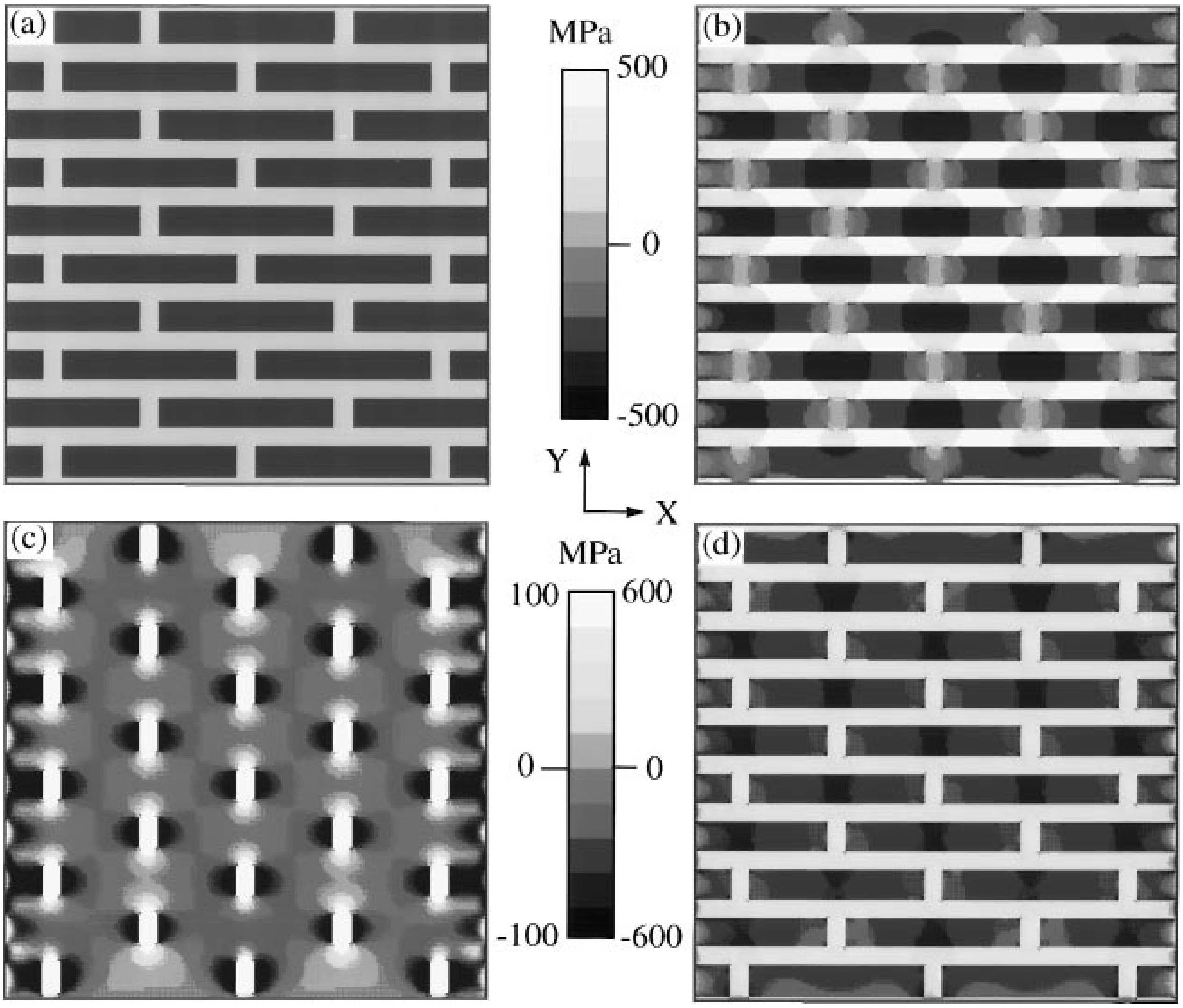

Figure 4 (a) The morphology, (b) residual thermal stress σ_x, (c) residual thermal stress σ_y, and (d) stress invariant, $\sigma_x + \sigma_y$, for brick wall-array grains with an intergranular phase.

becomes compressive in the intergranular layer parallel to the x-direction (Fig. 2c). The square grains are always in compression in both the x- and the y-directions. The stress invariant, $\sigma_x + \sigma_y$, is compressive in square grains, and is tensile in the intergranular layer (Fig. 2d). In square grains, it is noted that the stress invariant is more compressive at grain corners. Also, in the intergranular layer, the stress invariant is less tensile at the junction between the horizontal and the vertical intergranular layers.

For hexagon-array grains (Fig. 3a), the intergranular layers either are in the x-direction or incline at an angle of 30° with respect to the y-direction. It can be seen in Fig. 3b that σ_x is more tensile in the horizontal intergranular layer than in the inclined intergranular layer, and compression in the intergranular layer can be observed in the region adjacent to the grain corner pointing in the x-direction. The distributions of σ_y shown in Fig. 3c are different from those of σ_x (Fig. 3b). Whereas σ_y is tensile in the inclined intergranular layer, it is compressive in the horizontal intergranular layer. The stress invariant, $\sigma_x + \sigma_y$, is compressive in hexagonal grains, and is tensile in intergranular layers (Fig. 3d). In the intergranular layer, the stress invariant is less tensile at the junction between the horizontal and the inclined intergranular layers.

For brick wall-array grains (Fig. 4a), the intergranular layers are oriented in either the x- or the y-direction. However, while horizontal intergranular layers are continuous, the vertical intergranular layers consist of short segments. It can be seen in Fig. 4b that σ_x is tensile in the intergranular layer; however, it is more tensile in the horizontal intergranular layer. In the elongated grain, σ_x is more compressive in the central region of the grain which is in consistent with a recent stress-transfer analysis [13]. Fig. 4c shows that σ_y is tensile in the vertical intergranular layer but is compressive in the horizontal intergranular layer. Compared to σ_x, σ_y has a much smaller magnitude in the system (see Tables II and III). The stress invariant, $\sigma_x + \sigma_y$, is compressive in elongated grains, and is tensile in intergranular layers (Fig. 4d).

3.2. Residual stresses in an actual microstructure

A micrograph is converted to a *ppm* format, and the digitized image is shown in Fig. 5a, in which random

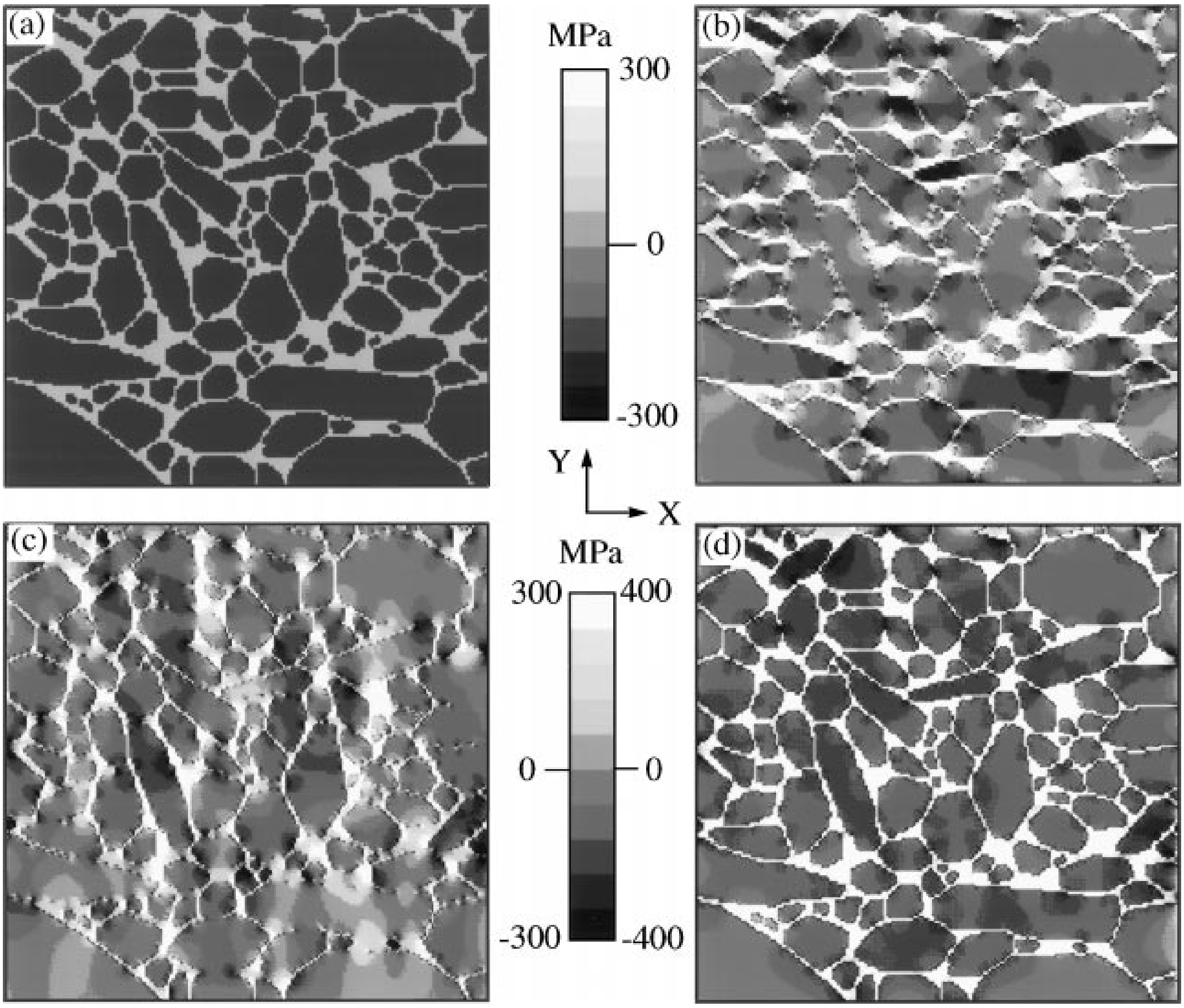

Figure 5 (a) The digitized micrograph, (b) residual thermal stress σ_x, (c) residual thermal stress σ_y, and (c) stress invariant, $\sigma_x + \sigma_y$, for an actual microstructure of random-array grains with an intergranular phase.

distribution of isolated grains are surrounded by a continuous intergranular phase. The area fraction of intergranular phase in Fig. 5a is ~0.22. Using *OOF*, the calculated stress maps for σ_x, σ_y, and $\sigma_x + \sigma_y$ are shown in Fig. 5b–d, respectively. Statistical summaries of residual stresses in the grains and the intergranular phase are also listed in Tables II and III, respectively. For σ_x, it can be seen in Fig. 5b that the region of higher tension in the intergranular phase (i.e., the lighter color) and the region of higher compression in grains (i.e., the darker color) tend to orient in the x-direction. Similarly, Fig. 5c shows that the region of higher tension in the intergranular phase and the region of higher compression in grains tend to orient in the y-direction for σ_y. The stress invariant, $\sigma_x + \sigma_y$, is compressive in grains, and is tensile in the intergranular phase (Fig. 5d).

3.3. Effective CTEs

Whereas residual thermal stresses can be obtained directly from the simulated results, effective CTEs are obtained by the following procedures. First, the elastic strains in the x- and the y-directions are averaged for all elements. Division of the average elastic strains by ΔT signifies the deviation of the effective CTEs from the rule-of-mixtures CTE, α_{rom}. Then, the effective CTEs in the x- and y-directions, α_x^* and α_y^*, are obtained by adding their deviations to α_{rom}.

Using Equations 10, the predicted effective CTE, α^*, from analytical modeling is shown in Fig. 6. The rule-of-mixtures CTE, α_{rom}, is also shown. The negative deviation of α^* from α_{rom} is because the grains has a higher Young's modulus but a lower CTE than the intergranular phase. The calculated α_x^* and α_y^* based on the microstructures depicted by Figs 2a, 3a, 4a, and 5a are shown in Fig. 6. Additional results for the three model microstructures with a different area fraction of intergranular phase than that in Figs 2a, 3a, and 4a are also added. For square-array grains, $\alpha_x^* = \alpha_y^*$ and only one data is shown for each intergranular phase content which is in excellent agreement with the effective CTE predicted from analytical modeling. For other arrays, $\alpha_x^* \neq \alpha_y^*$; however, the difference between α_x^* and α_y^* is negligible for hexagon-array grains. While α_x^* and α_y^* show only small deviation from α^* for hexagon-array and random-array grains, they deviate significantly from α^* for brick wall-array grains. Hence, the microstructure with aligned elongated grains has significant anisotropic CTEs. The effective CTEs for unidirectional fiber-reinforced ceramics have previously been analyzed by using a composite-cylinder model [9]. It is shown in Fig. 7 that α_x^* and α_y^* for brick

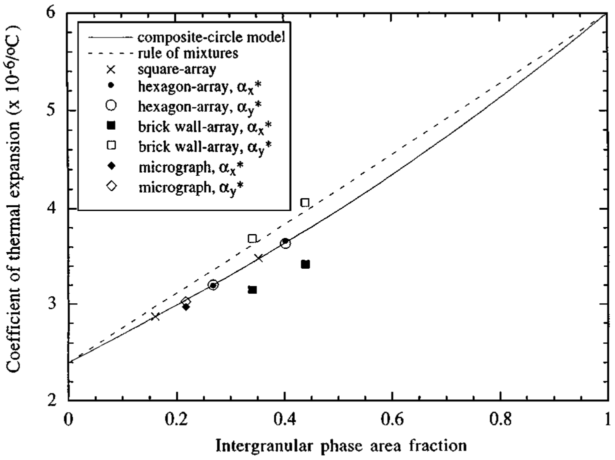

Figure 6 Effective CTEs predicted from analytical modeling and numerical simulations.

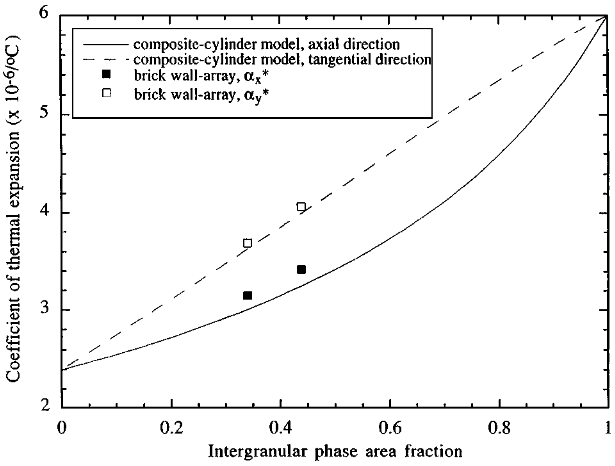

Figure 7 Effective CTEs in the axial and the tangential directions predicted from a composite-cylinder model, and α_x^* and α_y^* obtained from two-dimensional numerical simulations of brick wall-array grains with an intergranular phase.

wall-array grains agree well, respectively, with the prediction of the effective CTEs in the axial and the tangential directions using the composite-cylinder model (see Equations 8b and 8a in Ref. 9) despite the difference between two-dimensional and three-dimensional geometries.

4. Concluding remarks

Residual thermal stresses and effective CTEs of intergranular two-phase composites were analyzed in a two-dimensional sense. The system consists of isolated grains and a continuous intergranular phase. Both analytical modeling and numerical simulations were used to analyze the system. While a composite-circle model was adopted in analytical modeling, model microstructures of square-array, hexagon-array, and brick wall-array grains with an intergranular phase as well as an actual microstructure of random-array grains with an intergranular phase were adopted for numerical simulations. The following results were concluded.

- Unless the grains are elongated and aligned (Fig. 4), the effective CTEs can be well predicted using a simple composite-circle analytical model. The aligned elongated grains induce significant anisotropic effective CTEs in the two-phase composite.
- The difference between the effective CTE, α^* (Equation 10), predicted from analytical modeling and the rule-of-mixture CTE, α_{rom} (Equation 11), depends mainly on the Young's modulus ratio between the two phases. When the two phases have the same elastic constants, $\alpha^* = \alpha_{\mathrm{rom}}$. Otherwise, α^* shifts away from α_{rom} in the direction of the CTE of the harder phase. However, α_{rom} can be used in general to predict the effective CTE of a two-phase composite unless the two phases have very different Young's moduli.
- When the intergranular phase has a greater CTE than the isolated grain, the intergranular phase and the grain are subjected to hydrostatic tension and compression, respectively. In the intergranular phase, it is noted that the hydrostatic stress is less tensile in the region of multiple grain junction. Also, the stress component has the highest tension in the direction parallel to the grain boundary and can even become compressive in the direction normal to the grain boundary.

Acknowledgments

The authors thank Ms. S. B Waters for processing the micrograph (Fig. 5a), and Drs. M. J. Lance and X. L. Wang for reviewing the manuscript. Research sponsored by the U.S. Department of Energy, Division of Materials Sciences, Office of Basic Energy Sciences, under contract DE-AC05-96OR22464 with Lockheed Martin Energy Research Corp.

References

1. M. P. HARMER, H. M. CHAN and G. A. MILLER, *J. Am. Ceram. Soc.* **75** (1992) 1715.
2. M. TAYA, S. HAYASHI, A. S. KOBAYASHI and H. S. YOON, *ibid.* **73** (1990) 1382.
3. K. NIIHARA, *J. Ceram. Soc. Jpn.* **99** (1991) 974.
4. I. M. PETERSON and T. Y. TIEN, *J. Am. Ceram. Soc.* **78** (1995) 2345.
5. R. A. SCHAPERY, *J. Compos. Mater.* **2** (1968) 380.
6. B. W. ROSEN, *Proc. R. Soc. London A* **319** (1970) 79.
7. D. K. HALE, *J. Mater. Sci.* **11** (1976) 2105.
8. N. LAWS, *Int. J. Eng. Sci.* **12** (1974) 79.
9. C. H. HSUEH and P. F. BECHER, *J. Am. Ceram. Soc.* **71** (1988) C438.
10. S. A. LANGER, W. C. CARTER and E. R. FULLER, "Object Oriented Finite Element Analysis for Materials Science" (Center for Theoretical and Computational Materials Science and the Information Technology Laboratory at the National Institute of Standards and Technology, 1997).
11. S. P. TIMOSHENKO and J. N. GOODIER, "Theory of Elasticity" (McGraw-Hill, New York, 1951) p. 69.
12. P. F. BECHER, E. Y. SUN, C. H. HSUEH, K. B. ALEXANDER, S. L. HWANG, S. B. WATERS and C. G. WESTMORELAND, *Acta Metall. Mater.* **44** (1996) 3881.
13. C. H. HSUEH, E. R. FULLER, S. A. LANGER and W. C. CARTER, "Analytical and Numerical Analyses for Two-Dimensional Stress Transfer," *Mater. Sci. Eng.* **A268** (1999) 1.

Received 17 March 1999
and accepted 2 June 2000